EXPLORING THE CLIMATIC IMPACT OF BI-MODAL DUST PARTICLE SIZE DISTRIBUTIONS DURING THE MY34/2018 GLOBAL DUST STORM WITH THE NASA AMES MARS GLOBAL CLIMATE MODEL

R. A. Urata, *Bay Area Environmental Research Institute, Moffett Field, CA, USA (richard.a.urata@nasa.gov)*, **T. Bertrand**, *LESIA, Paris Observatory, France*, **M. A. Kahre, R. J. Wilson**, *NASA Ames Research Center, Moffett Field, CA, USA*, **A. M. Kling**, *Bay Area Environmental Research Institute, Moffett Field, CA, USA*, **Mike Wolff**, *Space Science Institute, Boulder, CO, USA.*

Introduction: The 2018 Global Dust Storm (GDS) has been observed on Mars from the surface and from orbit. Recent modeling efforts of the 2018 GDS highlight that climate models do not simultaneously capture both the evolution of surface temperatures, semi-diurnal tide amplitude, and the decay rate of global column dust opacities, which suggests that significant changes in dust particle sizes may occur during the dust storm (e.g., [1], [2]). These models typically assume a constant lifted dust particle size—with size evolution occurring in the atmosphere but only because of gravitational sedimentation. For instance, simulations with sufficiently large particles sizes to produce reasonable decay/sedimentation rates also produce excessive infrared radiation at the surface, with excessively warm surface temperatures during peak dust loading (Fig. 1).

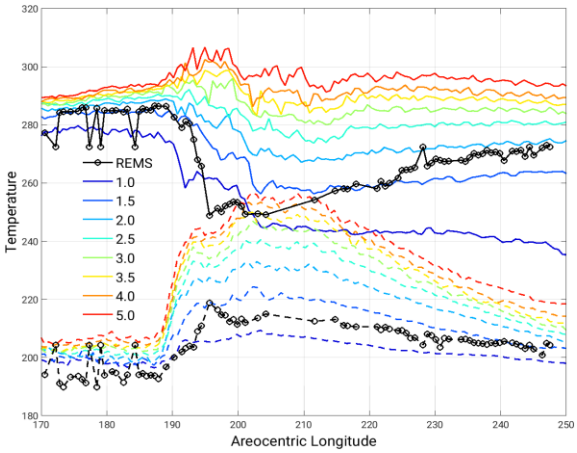

Figure 1. Diurnal max and min surface temperatures near the Curiosity lander site with various constant lifted dust particle size.

One possible way to improve the agreement between the simulations and the observations is to allow the dust particle sizes to change more significantly in time and/or space during the simulated GDS. Particle size evolution toward larger radius during GDSs is supported by several observations (e.g., [3], [4]). Different mechanisms could take place during dust storms to shift the dust particle distribution towards a larger effective radius, including: (1) the lifted particle size at the surface could change due to different active reservoirs or due to depletion of small particles as the storm increases in intensity and (2) the particle size in the atmosphere could change more significantly due to Brownian coagulation (production of large particles by the collisions induced by Brownian motions of the particles in the gas and subsequent sticking together of small particles), or gravitational coagulation (accretion through sedimentation; [5], [6], [7], [8]). Previous 1-D studies have explored the impact of coagulation processes and concluded that coagulation only affects smaller particles (<0.1 micron) and only changes dust opacities by a few percent during dust storms (e.g., [5]). We have previously explored this with a GCM and found that it allowed for a better decay phase with smaller particles [9].

Here we use the NASA Ames Mars Global Climate Model (MGCM) to investigate these processes during the 2018 Global Dust Storm. We build our investigation upon the previous modeling of the GDS performed with a uniform lifted effective particle radius [1]. That study revealed that the dust number density during the dust storm is ~10 times higher than during non-storm conditions, and should thus favor coagulation processes. We will show how these mechanisms impact the evolution of particle sizes, dust distributions, surface and atmospheric temperatures, and tidal components throughout the GDS.

Methods: The NASA Ames MGCM is a global climate model with Mars physics partially developed for the Legacy Mars GCM over the past few decades (e.g., [10]), and the FV3 dynamical core from NOAA/GFDL [11]. The FV3 dycore uses a cubed-sphere horizontal grid which avoids the converging meridians problem by remapping six faces of a cube to a sphere. Horizontal and vertical resolutions are highly variable. Here we use 24 grid cells per cube face side, and 28 vertical layers. This corresponds to a horizontal resolution of approximately 240 km with a model top at approximately 0.05 Pa. Aerosol tracers are assumed to have log-normal distributions and are represented using the two-moment method, tracking mass and number.

Multiple dust modes. Terrestrial dust lifting is typically modeled using multiple modes (e.g., [12], [13]). Bimodal dust distributions have been suggested for Mars while climate models typically use single modes to represent dust. Observations suggest that the number density of the small mode is 25-100x higher than the large mode, while the mass of the

small mode is 1-50x less than the large mode ([7], [8], 14], [15]).

In this study we present a **self-consistent model** for multiple modes of dust. Each mode is treated as a separate tracer, tracking mass and number for each mode. The mass fraction of dust in each mode that is lifted is an input parameter, from which the amount of dust lifting is calculated so that the simulated dust column opacity follows the observations (Daily Global Dust Maps, [2]). Although these modes are treated independently for advection and sedimentation, there are physical processes where the modes must be considered simultaneously, including the total dust opacity for radiation and coagulation rates. The total dust extinction of a layer of atmosphere is $\tau_{ext} = A_0 Q_{ext} \Delta P/g$. Where $A_0 = \pi N_0 R_s^2$, the total cross-sectional area of dust particles (N_0 is the number mixing ratio), Q_{ext} is the extinction efficiency, and $\Delta P/g$ is the thickness of the layer. First, the mass and number moments of each mode are converted to a 20-bin normalized number density distribution, n_i. The total extinction efficiency (and other optical properties) are calculated by multiplying, for each bin, $Q_{ext,i}*n_i$ (assuming Mie scattering) and performing a summation over bins [10]. In order to find the combined contribution to optical properties from all modes, n_i is scaled by $A_{0,i}/A_{0,tot}$, the total cross-sectional area of each mode divided by the total cross-sectional area of all modes, and an additional sum over modes is performed to find the normalized number density weighted by cross-sectional area of each bin. An example of these distributions for varying fractions of a 0.3 μm mode and 3.0 μm mode is shown in Figure 2.

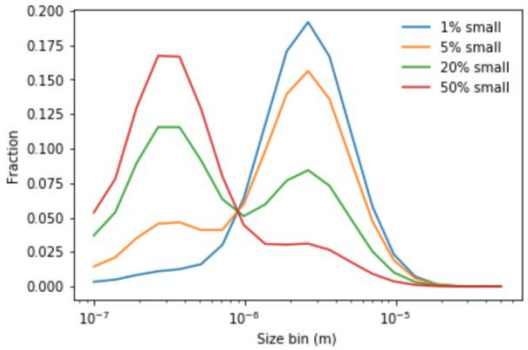

Figure 2. Normalized number density weighted by cross-sectional area of each bin ($n_i*A_{0,i}/A_{0,tot}$). This illustrates how the radiative transfer sees the lifted bimodal distributions for a 0.3 μm mode and 3.0 μm mode with 1%, 5%, 20%, and 50% small modes.

The coagulation combines the particle number of all modes to a single multi-modal distribution over bins then calculates coagulation rates according to equations from [16]. Following the coagulation rate calculation, the total distribution is split back into the original modes according to the original fraction of number for each mode to the total.

Results: We have performed simulations of the Mars Year 34 global dust storm with bimodal dust lifting of a 0.3 μm mode and a 3.0 μm mode with varying fractions of small and large modes. We compare these results to a default simulation using a single dust mode with an effective radius of 3.0 μm. The model is run following the Mars Year 34 dust climatology from [2] at 9.6 μm. The model is typically warm started from a spun-up phase, and we analyze results from the period of the year surrounding the global dust storm.

Mean dust opacity. We show the mean dust opacity for the latitudes 50° S to 50° N in Figures 3 and 4 for various dust scenarios compared to the reference climatology. Figure 3 shows the mean dust opacity in the reference infrared (IR) band at 9.6 μm, while Figure 4 shows the ratio of the reference visible (VIS) band at 0.67 μm to the reference IR band.

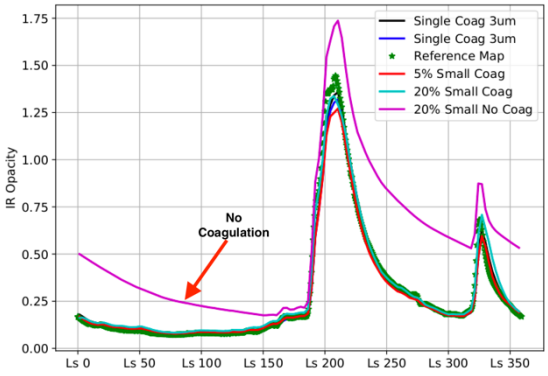

Figure 3. Latitudinal mean (50° S to 50° N) IR dust opacity for single mode (with and without coagulation), reference climatology, 5% small mode, and 20% small mode with and without coagulation.

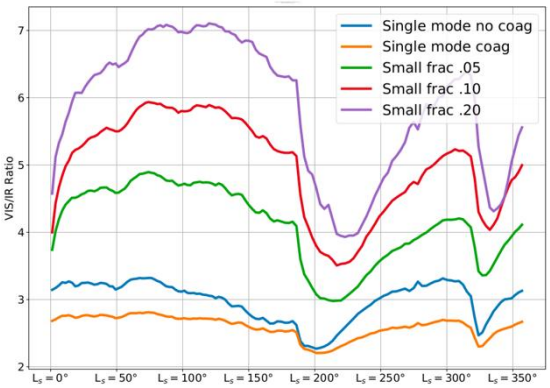

Figure 4. Latitudinal mean (50°S to 50°N) VIS/IR opacity ratio for single mode (with and without coagulation), 5% small mode, 10% small mode, and 20% small mode.

The model IR dust opacity is constrained by the reference IR dust map, and the model largely follows the reference opacity for most of the year except for the peak of the dust storm for the single mode case as well as the bimodal cases. However, coagulation must be considered in the bimodal cases or else the

small mode will not sediment at a sufficient rate and will lead to unrealistic dust loading and slower storm decay phase than observed. Lifting a modest amount of the small mode of dust can dramatically increase the VIS/IR opacity ratio compared to a single large mode, and can also impact the amplitude of the change in ratio over the annual cycle.

Equatorial zonal mean temperature. Lifting the small mode dust allows dust to reach higher altitudes in the atmosphere, as seen in Figure 5. This shows the dust mass mixing ratio (ppm) difference between the bimodal lifted dust and the single lifted mode during the global dust storm at L_s=210° with the mass streamfunction difference between the two cases overlayed. The bimodal case has significantly more dust aloft compared to the single mode case. This might be attributed to the rising branch of the Hadley cell in the bimodal case being able to lift up the smaller mode of dust more effectively. The effect of the increased dust mass aloft is apparent in the equatorial zonal mean temperature vertical time slices. Figures 6 and 7 show the equatorial zonal mean temperature versus time for a single dust mode of 3.0 μm (Fig. 6) and difference between a bimodal lifted dust distribution of 0.3 μm and 3.0 μm at 20% small mode and a single 3.0 μm mode (Fig. 7).

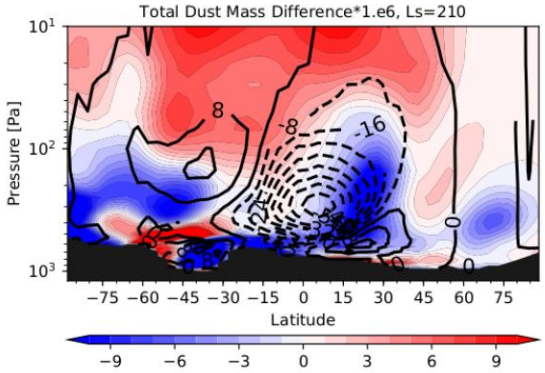

Figure 5. Zonal mean dust mass mixing ratio difference between bimodal lifted (0.3 μm and 3.0 μm dust, 20% small mode) minus single lifted 3.0 μm dust mode at L_s=210°. The zonal mean mass streamfunction difference is overlayed.

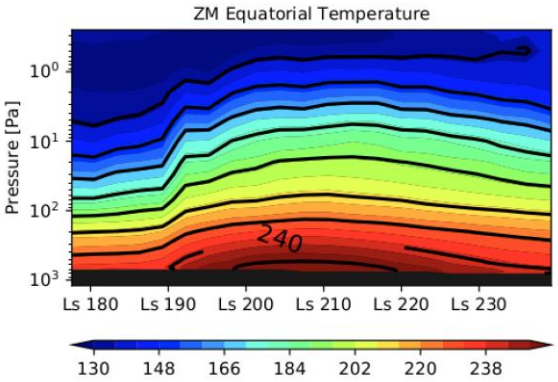

Figure 6. Zonal mean equatorial temperature for single lifted 3.0 μm dust mode.

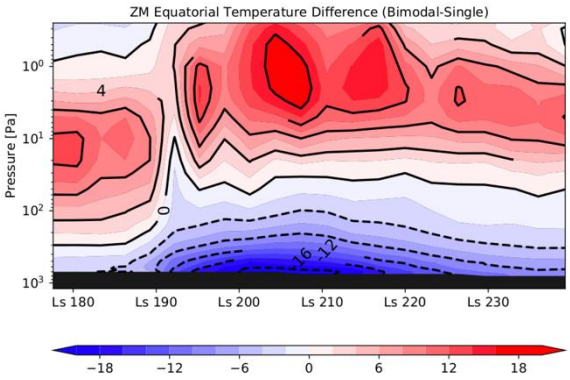

Figure 7. Zonal mean equatorial temperature difference between bimodal lifted (0.3 μm and 3.0 μm dust, 20% small mode) minus single lifted 3.0 μm dust mode.

Using the bimodal dust distribution for lifted dust tends to increase temperatures at higher altitudes, while decreasing temperatures near the surface. This is especially strong during the global dust storm that begins around L_s=190°, where 10 Pa temperatures are ~10 K warmer in the bimodal case during this period (Fig 7).

REMS temperature comparison. A key factor in the hypothesis for evolving particle sizes is the REMS surface temperature observations during the global dust storm [17]. During onset of the global dust storm there is a sudden drop in the diurnal surface temperature cycle amplitude, and a gradual recovery during the decay phase. A single constant dust mode cannot reproduce the daytime surface temperature drop at the onset, while smaller particles do not sediment quickly enough during the decay phase (Fig. 1) and do not match observations of dust particle sizes (e.g., [4]).

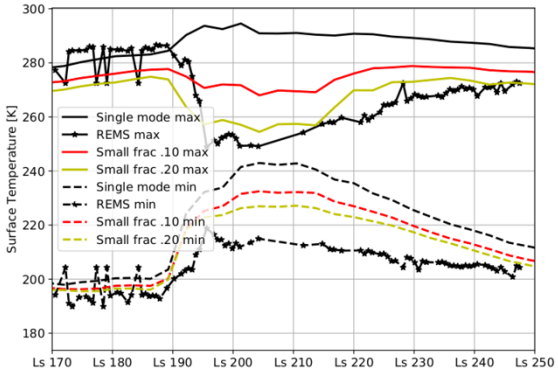

Figure 8. Diurnal max and min surface temperatures for REMS, and GCM near the Curiosity landing site for single mode, and 5%, 10%, 20% small mode.

Figure 8 shows the diurnal max and min surface temperatures from REMS, compared to the GCM near the Curiosity landing site for a single 3.0 μm mode, alongside 5%, 10%, and 20% small modes. Including a small mode to be lifted with a large

mode has a significant impact on the surface temperature diurnal cycle, while not dominating the mass of dust in the atmosphere. Following the global dust storm, the large mode tends to sediment more rapidly than a single small mode, while the small mode removal is assisted by coagulation creating larger particles. The model does not replicate the REMS surface temperatures precisely. However, the discrepancy between the dust climatology map and Curiosity dust opacity is well-documented [2], and a modified map may lead to a closer match.

Semi-diurnal tide response. The semi-diurnal (S2) tide calculated from the pressure observations from the REMS instrument is significantly impacted by the bimodal lifting of dust. Unlike the surface temperature which is highly dependent on local parameters such as albedo, thermal inertia, and the dust vertical distribution, the S2 tide is more responsive to global forcing. A comparison between the simulated and observed S2 tide is shown in Figure 9.

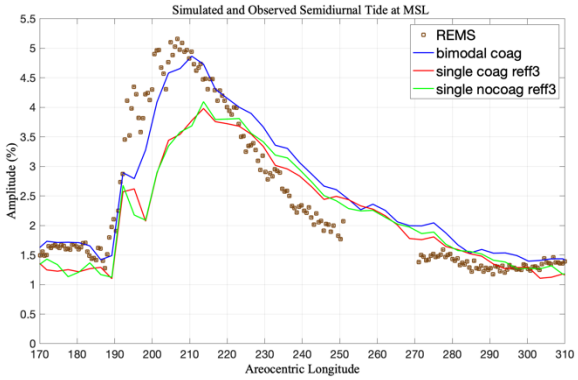

Figure 9. Semi-diurnal tide comparison between observed, single lifted 3.0 μm dust mode with and without coagulation, and bimodal lifted (0.3 μm and 3.0 μm dust, 20% small mode) simulations.

The observed S2 tide appears to be a reliable approximation of the migrating S2 tide which is a robust measure of the globally-integrated aerosol thermal forcing, particularly during the decay of the storm after L_s=205°. This is a consequence of the meridionally broad and vertically deep character of the dominant Hough function (from classical tide theory) excited by globally distributed aerosol heating. The migrating diurnal tide estimate appears to be sensitive to the vertical distribution of dust, which depends on the lifted particle size distribution. As shown in Figure 9, the bimodal dust case fits the S2 tide response better than the single constant dust mode cases.

Conclusions: We have demonstrated the sensitivity of the climate to the inclusion of a second, smaller mode of dust. Using a self-consistent bimodal dust lifting scheme with a minor fraction of a small mode leads to an improvement in areas such as the diurnal surface temperature cycle during the global dust storm. Dust tends to be lifted through a deeper column in the atmosphere, and the surface temperatures reflect the smaller particles. The observed tides at MSL will also be an important basis for evaluating our simulations of evolving particle size, as the tidal response has been shown to be sensitive to vertical dust distribution, and thus the lifted distribution. Future work will constrain model parameters such as the effective radii of modes and the fraction of each mode lifted by performing comparisons to observations. Observations of atmospheric temperatures, brightness temperatures, dust particle size retrievals, or indirect indications of the particle sizes such as the VIS/IR dust opacity ratio.

References:

[1] Bertrand, T., et al. (2020). *Journal of Geophysical Research: Planets*, 125, e2019JE006122. https://doi.org/10.1029/2019JE006122

[2] Montabone, L., et al. (2020). *Journal of Geophysical Research: Planets*, 125, e2019JE006111. https://doi.org/10.1029/2019JE006111

[3] Elteto, A., & Toon, O. B. (2010). *Icarus, 210*(2), 589–611. https://doi.org/https://doi.org/10.1016/j.icarus.2010.07.011

[4] Lemmon, M. T., et al. (2019). *Geophysical Research Letters*, 46, 9448– 9456. https://doi.org/10.1029/2019GL084407

[5] Murphy, J. R., et al. (1990). *Journal of Geophysical Research*, 95, p. 14629-14648.

[6] Jacobsen, M.Z. (1999). Fundamentals of Atmospheric Modeling. Cambridge Univ. Press. 656.

[7] Montmessin, F., P. Rannou, and M. Cabane, (2002), *Journal of Geophysical Research*, **107**(E6), 5037, doi:10.1029/2001JE001520

[8] Fedorova, A. A., et al. (2014). *Icarus, 231*, 239–260. https://doi.org/10.1016/j.icarus.2013.12.015

[9] Bertrand, T., et al. (2021). Europlanet Science Congress. doi:10.5194/espc2021-585.

[10] Haberle, R. M., et al. (2019). *Icarus, 333*. https://doi.org/10.1016/j.icarus.2019.03.026

[11] Putman, W. M., Lin, S. J. (2007). *Journal of Computational Physics, Volume 227, Issue 1*. https://doi.org/10.1016/j.jcp.2007.07.022.

[12] Weinzierl, et al. (2009). *Tellus, Series B: Chemical and Physical Meteorology*, *61*(1), 96–117. https://doi.org/10.1111/j.1600-0889.2008.00392.x

[13] Ryder, C. L., et al. (2013). *Atmospheric Chemistry and Physics*, *13*(1), 303–325. https://doi.org/10.5194/acp-13-303-2013

[14] Luginin, M., et al. (2020). *Journal of Geophysical Research: Planets*, e2020JE006419. https://doi. org/10.1029/2020JE006419

[15] Shaposhnikov, D. S., et al. (2018). *Journal of Geophysical Research: Planets*, 123. https://doi.org/10.1002/2017JE005384

[16] Jacobson, M. Z., et al. (2005). *Environmental Science & Technology*, *39*(24), 9486–9492. https://doi.org/10.1021/es0500299

[17] Guzewich, S. D., et al. (2019). *Geophysical*

Research Letters, 46, 71–79.